Available online at www.sciencedirect.com
ScienceDirect
Comput. Methods Appl. Mech. Engrg. 412 (2023) 115996
Computer methods in applied mechanics and engineering
www.elsevier.com/locate/cma

The *a posteriori* finite element method (APFEM), a framework for efficient parametric study and Bayesian inferences

Yanis Ammouche, Antoine Jérusalem*

Department of Engineering Science, University of Oxford, Parks Road, Oxford, OX1 3PJ, UK

Received 6 November 2022; received in revised form 7 March 2023; accepted 9 March 2023
Available online 19 May 2023

Dataset link: https://github.com/muphisim

Abstract

Stochastic methods have recently been the subject of increased attention in Computational Mechanics for their ability to account for the stochasticity of both material parameters and geometrical features in their predictions. Among them, the Galerkin Stochastic Finite Element Method (GSFEM) was shown to be particularly efficient and able to provide accurate output statistics, although at the cost of intrusive coding and additional theoretical algebraic efforts. In this method, distributions of the stochastic parameters are used as inputs for the solver, which in turn outputs nodal displacement distributions in one simulation. Here, we propose an extension of the GSFEM—termed the *A posteriori* Finite Element Method or APFEM—where uniform distributions are taken by default to allow for parametric studies of the inputs of interest as a postprocessing step after the simulation. Doing so, APFEM only requires the knowledge of the vertices of the parameter space. In particular, one key advantage of APFEM is its use in the context of Bayesian inferences, where the random evaluations required by the Bayesian setting (usually done through Monte Carlo) can be done exactly without the need for further simulations. Finally, we demonstrate the potential of APFEM by solving forward models with parametric boundary conditions in the context of (i) metamaterial design and (ii) pitchfork bifurcation of the buckling of a slender structure; and demonstrate the flexibility of its use for Bayesian inference by (iii) inferring friction coefficient of a half plane in a contact mechanics problem and (iv) inferring the stiffness of a brain region in the context of cancer surgical planning.

Keywords: Stochastic finite element method; Bayesian inferences; Parameter space exploration

1. Introduction

Engineers have traditionally been relying on forward mathematical models—i.e., models where kinematic and mechanical outputs are provided for a given set of inputs, typically material properties and boundary conditions—such as the finite element method to describe the mechanical behaviour of physical systems. While such approaches have reached an exceptional maturity, they remain inadequate for applications where model parameters may be partially or fully unknown. Unfortunately, such restricted knowledge is ubiquitous in virtually all fields related to mechanics. In the aerospace and automotive industries, for example, fibre reinforced polymer composites (FRPC)

* Corresponding author.
E-mail address: antoine.jerusalem@eng.ox.ac.uk (A. Jérusalem).

https://doi.org/10.1016/j.cma.2023.115996

are widely used because of their high strength and light weight. The main moulding methods for FPRC, however, all introduce imperfections in the matrix, fibre and/or the interface, in turn leading to misalignment, waviness and uneven spatial distribution of the fibres and delamination between layers, thus making deterministic simulations unreliable [1]. Similarly, the relatively recent, albeit stratospheric, progress in additive manufacturing (AM) has been hampered by strong geometrical deviations compared to the original target design [2]. These imperfections in the material properties and structural characteristics essentially undermine any guarantee that deterministic analyses can offer reliable predictions of mechanical behaviours for AM made structures, such as, among others, lattice-based architected materials (e.g., metamaterials).

The most straightforward approach to account for these uncertainties is the Monte Carlo (MC) method, where the forward model is repeatedly evaluated to obtain statistics of the model predictions after sampling a given number of stochastic input parameter realisations. This approach, however, suffers from a slow convergence rate in $O(N^{-0.5})$ [3], making the time and computational cost prohibitive for high fidelity systems. To alleviate this issue, other alternatives involving polynomial chaos expansion (PCE), first introduced by Weiner [4], are also used. They consist of rewriting any given output (e.g., stress, displacement) as a PCE polynomial surrogate whose coefficients have to be determined. Initially, Weiner used Hermite polynomials of random variables and achieved exponential convergence for gaussian random variables. Later, Ref. [5] extended this framework to other input distributions. There are two leading methodologies to obtain PCE coefficients. The first type is non intrusive and requires running simulations at given input parameter collocation points. The coefficients are then determined by solving a least-square problem [6]. The choice of collocation points has an important impact on the accuracy of the results [7] and is sometimes *ad hoc* [8]. The second type, intrusive, performs a Galerkin projection on the stochastic dimension to obtain the unknown PCE coefficients [9,10], the so-called Galerkin stochastic finite element method (GSFEM). This intrusive approach leads to a reformulation of the governing equations and important coding efforts, though algebraic operations have been proposed to alleviate this issue [11,12] and other polynomials interpolants have been proposed to capture singularities [12,13].

One drawback of probabilistic methods is that they require knowledge of the probabilistic distributions of input parameters. However, obtaining probability distributions requires an extensive amount of data, sometime difficult or costly to gather. Furthermore, in most realistic cases, only physical parameter bounds are known. Hence, non-probabilistic approaches have been developed considering only the bounds of the non-deterministic values. These approaches include interval methods as extensively described in the literature [14,15]. Interval methods infer the worst-case response of a given structure. Rao and coworkers [16] determined the crisp bounds of stress in beam structures with uncertainties on the cross-sectional area and the Young's modulus. Modares et al. [17] computed exact estimations of natural frequencies' extrema in structures with bounded uncertainties on the Young's modulus. Long et al. [18] computed the life bounds of a turbine generator rotor with a crack, and could predict effectively worst and best case scenarios for fatigue crack growth with uncertain knowledge of fracture toughness and initial crack length. This method was modified to be more efficient in case the model response is monotonic with respect to the input parameters [15,19]. Researchers have also extended the interval finite element analysis to model spatially uncertain fields [20]. In spite of their low computational cost, these methods can be over-conservative [15]. Furthermore, as only the extrema are derived, no insights are provided on the response of the model within the bounded parameter space, and these methods cannot be used when the data is excessively noisy.

When direct parameter identification is impossible, novel approaches solely accounting for the original (experimental) data have been proposed. The data-driven methodology of Ortiz and coworkers, formulating the problem as a minimisation of the distance function defined by the laws of conservation directly on observed (e.g., measured) output quantities, has already been applied to a wealth of applications [21–24]. Alternatively, bayesian inference (BI) has been used to extract the probability distributions of unknown inputs from external (e.g., experimental) output observations. Doing so, it allows for the estimation of internal parameters or quantities not directly available through external observations. Bayesian approaches have been used in various applications ranging from biophysics [25] and epidemic dynamics [26] to solid mechanics [27,28]. Fast and accurate Bayesian estimation is tightly related to the forward propagation efficiency of uncertainties as BI can require a high number of likelihood evaluations for different values of the model parameters, a highly time-consuming task. To this end, Rosic et al. [29] used PCE-based GSFEM to quantify random field properties in elasto-plastic problem with low computational cost, as suggested by previous research emphasising the potential of GSFEM for inverse analyses [30]. The restriction to PCE in this work does not, however, allow for the consideration of a wider range of applications where singularities are expected.

Here, we specialise our previously proposed GSFEM to uniform distributions to simultaneously obtain the detailed information of probabilistic methods, while only needing the knowledge parameter bounds. This approach avoids the pitfalls of the interval methods as it still captures the problem behaviour in-between, while leveraging the flexibility of the GSFEM in terms of both continuous (PCE interpolation) and discontinuous (wavelet interpolation) behaviours. It is important to note that this does not mean that the real parameter distribution is required to follow a uniform distribution. Instead, and as opposed to GSFEM, the proposed framework, termed *A posteriori* Finite Element Method or APFEM, is aimed at being used as an *a posteriori* exploratory tool for parameter optimisation or Bayesian inference (BI) without the need to run multiple simulations. In the following, we propose the theoretical framework, and demonstrate its relevance and flexibility in the context of metamaterial's optimisation, multi-directional buckling prediction, as well as two BI problems: the determination of friction coefficient of a half plane in a contact mechanics problem based on observable displacements of the outer boundaries, and the determination of the stiffness of brain tumour in the context of clinical planning based on the measurements of the midline shift during a rise of vascular pressure.

2. General framework

This section briefly recalls the mathematical foundation of the GSFEM, specialises it to the APFEM and recalls the formulation of BI for inverse problems.

2.1. APFEM

The APFEM is the application of the GSFEM to the case where input distribution follows a uniform distribution. Such a distribution ensures optimal exploration of the stochastic parameter space.

2.1.1. GSFEM

The GSFEM decomposes any given stochastic quantity on a space generated by a set of interpolants Ψ_ϵ, or stochastic shape functions. Displacements, among other quantities, are characterised by deterministic nodal and stochastic components. As an example, the finite element displacement function $\boldsymbol{u}$ is written as follows:

$$\boldsymbol{u}(\boldsymbol{x},\boldsymbol{\theta}) = \sum_a N_a(\boldsymbol{x})\boldsymbol{u}^a = \sum_a N_a(\boldsymbol{x}) \sum_\epsilon \Psi_\epsilon(\theta)\boldsymbol{u}^{a\epsilon}, \tag{1}$$

where the functions N_a are the usual finite element shape functions, Ψ_ϵ the shape functions associated to the stochastic space and $\boldsymbol{u}^{a\epsilon}$ the displacement of node a with stochastic direction ϵ.[1] The dependence on θ denotes a function on the probability space. Consequently, at a given node, both spatial and stochastic components of the displacement have to be determined. The choice of the stochastic shape functions depends on the probabilistic distribution of the inputs to ensure exponential convergence [5,31]. We term here the APFEM the specialisation of the GSFEM to inputs taken with uniform distribution. It must be emphasised that this does not mean that the real inputs necessarily follow a uniform distribution. Instead, it offers a flexible parameter (θ)—which can be chosen to vary between -1 and 1 without loss of generality—to be varied *a posteriori* in Eq. (1) to span the effect of the input parameter value change directly on the calculated nodal displacements. In essence, the stochastic parameter θ is used as a parametric parameter for input change effect exploration. Note also that the choice of uniform distribution weighs the finite element error equally over the entire (finite) parameter space, as opposed to other distribution, e.g., Gaussian, that penalises more the error near the mean of the parameter space. Consequently, all results obtained through the APFEM are expected to give accurate approximation of the model response for the whole range of input values (as opposed to favouring the most probable). In this case, Legendre polynomials are used for Ψ_ϵ to ensure optimal convergence [5,31].

We consider a multivariate random variable $\boldsymbol{\theta} = [\theta_1, \ldots, \theta_N]$, where $\theta_i \colon \Theta \to E$, $\forall i \in [1, N]$, with Θ the sample space of a probability triple (Θ, A, $\mathbb{P}$) with a σ-algebra A, probability measure $\mathbb{P}$, for a support E. We define $\mathbb{P}_{\boldsymbol{\theta}}$, the cumulative distribution function (CDF) of $\boldsymbol{\theta}$, as follows:

$$\mathbb{P}_{\boldsymbol{\theta}}(\boldsymbol{w}) = \mathbb{P}(\theta_1 \leq w_1, \ldots, \theta_N \leq w_N), \tag{2}$$

[1] Here and subsequently, indices noted with Greek letters relate to the stochastic space.

where $\boldsymbol{w} = [w_1, \ldots, w_N]$. The weak form of the balance of linear momentum can be formulated as follows: for all arbitrary admissible virtual stochastic displacement $\boldsymbol{\eta}$, with $\boldsymbol{\eta}(\boldsymbol{X}, \theta) = \boldsymbol{0}$ almost surely for all $\boldsymbol{X} \in \partial\Omega_d$, where $\partial\Omega_d$ represents the set where Dirichlet boundary conditions are applied,

$$\int_{E^N}\int_{\partial\Omega_n} \bar{\boldsymbol{T}}\cdot\boldsymbol{\eta}\,\mathrm{d}S\mathrm{d}\mathbb{P}_{\boldsymbol{\theta}}(\boldsymbol{w}) + \int_{E^N}\int_{\Omega_0}\rho_0\boldsymbol{b}\cdot\boldsymbol{\eta}\,\mathrm{d}V\mathrm{d}\mathbb{P}_{\boldsymbol{\theta}}(\boldsymbol{w}) = \int_{E^N}\int_{\Omega_0}\boldsymbol{P}:\mathrm{Grad}\,\boldsymbol{\eta}\,\mathrm{d}V\mathrm{d}\mathbb{P}_{\boldsymbol{\theta}}(\boldsymbol{w}) + \int_{E^N}\int_{\Omega_0}\rho_0\ddot{\boldsymbol{u}}\cdot\boldsymbol{\eta}\,\mathrm{d}V\mathrm{d}\mathbb{P}_{\boldsymbol{\theta}}(\boldsymbol{w}), \quad (3)$$

where $\boldsymbol{b}$ represents the body forces, ρ_0 the volumic mass, $\boldsymbol{T}$ the applied traction forces and $\boldsymbol{P}$ the first Piola–Kirchhoff tensor; all of these *a priori* stochastic in nature. The general details of the constitutive model definition, computation of tangent modulus and overall numerical implementation of GSFEM can be found in the work of Ammouche and Jérusalem [12].

2.1.2. Interpolants

This section covers briefly the two expansions used in this work, as originally described by Ammouche and Jérusalem [12].

2.1.2.1. Polynomial chaos expansion. The PCE was first introduced by Weiner [4] to create a surrogate that determines the evolution of uncertainty in a dynamical system. This metamodel is dependent on the probabilistic distribution of input parameters. Initially, Hermite polynomials were used for all distributions. According to the Cameron–Martin theorem [31], this expansion converges in the L_2 sense for a stochastic process with finite variance depending on Gaussian stochastic variables. Xiu and Karniadakis [5] established the optimal expansions for various probabilistic distribution of the inputs, including, for uniform distribution, the Legendre polynomials. As the APFEM only requires the use of uniform distribution, we detail the expression the Legendre polynomials of order n:

$$P_n(\theta) = \frac{1}{2^n}\sum_{k=0}^{n}\binom{n}{k}^2(\theta-1)^{n-k}(\theta+1)^k. \quad (4)$$

The univariate polynomials ψ's are proportional to the Legendre polynomials P_n. This multiplication factor is found by imposing the coefficient of the highest degree to 1 for each of the univariate polynomial.

Let us now consider $\boldsymbol{\theta} = [\theta_1, \ldots, \theta_N]$ a vector of uncorrelated random variables following an uniform probability distribution. The extension of univariate to M multivariate polynomials Ψ of the PCE on $\Theta_1 \times \cdots \times \Theta_N$ is defined as follows:

$$\Psi = \left\{ \prod_{i=1}^{N}\psi_{\lambda_i}(\theta_i) : \sum_{i=0}^{N}\lambda_i \leq n \right\}, \quad (5)$$

where λ_i refers to the order of the univariate polynomial associated to θ_i and where n indicates the degree of the expansion. The number of multivariate polynomials in a PCE expansion of order n is $M = \binom{n+N}{n}$. These expansions are suitable when the quantity of interest exhibits a smooth dependence on the input parameters.

2.1.2.2. Wavelet expansion. The PCE is not suitable when modelling outputs exhibiting discontinuous or sharp changes over the parameter space [12,13]. To alleviate this issue, we previously proposed here to use a wavelet expansion [12]. Haar expansions were first considered but were shown to be deficient in non-singular problems. Instead, the proposed wavelet expansion uses both continuous and discontinuous functions. In the following, we briefly recall its formulation and specialisation to uniform distributions.

A space V^N, containing polynomials of order equal to or smaller than N, is constructed with a cardinality of $N+1$. Typically, the scaled Legendre polynomials $[\phi_0, \ldots, \phi_N]$ are used as a basis of V^N. Discontinuous orthonormal functions $[\psi_0, \ldots, \psi_N]$ are then built as follows [32]:

(i) Two sets of polynomials $p_i(y)$ and $q_i(y)$ are defined:

$$\begin{cases} p_i(y) = y^i \\ q_i(y) = \begin{cases} p_i(y), & \text{if } 0 \leq y \leq 0.5 \\ -p_i(y), & \text{if } 0.5 < y \leq 1. \end{cases} \end{cases}$$

(ii) Each polynomial q_i is orthogonalised with respect to all the functions p_i to obtain a new set of polynomials $[\tilde{q}_0, \ldots, \tilde{q}_N]$;

(iii) Using a Gram–Schmidt scheme, the set of polynomials $[\tilde{q}_0, \ldots, \tilde{q}_N]$ are orthogonalised with respect to each other to give a set of polynomials $[r_0, \ldots, r_N]$;
(iv) The set of polynomials $[r_0, \ldots, r_N]$ is normalised to obtain the functions $[\psi_0, \ldots, \psi_N]$.

By construction, the functions ψ_i and ϕ_j are orthogonal. We define the functions ψ_{ik}^j as:

$$\psi_{ik}^j(y) = 2^{\frac{j}{2}} \psi_i(2^j y - k). \tag{6}$$

A given stochastic process is finally expanded using the following wavelet expansion:

$$X(y) = \sum_{i=0}^{N} X_i \phi_i(y) + \sum_{i=0}^{N} \sum_{j=0}^{n} \sum_{k=0}^{2^j-1} X_{i+(N+1)(2^j+k)} \psi_{il}^k(y). \tag{7}$$

The coordinates X_i, where $i = 0, \ldots, 2^{n+1}(N+1) - 1$, are obtained by projection of X along the functions ψ_{il}^k and ϕ_i. More information can be found about the underlying mathematical theory of these expansions in [13,32]. The variable y represents the CDF of the input parameters. For most probabilistic distributions, e.g., Gaussian distributions, the variable y does not have a closed form, which introduces inaccuracies in the numerical implementation of Eq. (7). This is not the case for univariate uniform distribution, where the CDF y can then be written as follows:

$$y(w) = \frac{w+1}{2} \tag{8}$$

where w is comprised between -1 and 1 and belongs to the support space of the uniform random variable. Extension to multivariate uniform distributions follows naturally.

2.2. Bayesian inferences

The principle of the Bayesian method is to deduce parameters of a model using observable quantities. While regression methods return a single value for each parameter using optimisation principles, BI estimates the probability distribution of inputs.

Let us assume a forward model describing the relationship between two multivariate random variables $\boldsymbol{X} = [X_1, \ldots, X_{N_{in}}]$ and $\widetilde{\boldsymbol{Y}} = [\tilde{Y}_1, \ldots, \tilde{Y}_{N_{out}}]$. Here, N_{in} and N_{out} are, respectively, the number of unknown parameters and the number of observable outputs. We define X_i: $\Theta \to E$ and $\tilde{Y}_j$: $\Theta \to \mathbb{R}$, $\forall i \in [1, N_{in}]$ and $\forall j \in [1, N_{out}]$, where the support E is $[-1,1]$. We then write:

$$\widetilde{\boldsymbol{Y}} = \boldsymbol{f}(\boldsymbol{X}). \tag{9}$$

Here, $\widetilde{\boldsymbol{y}}$ and $\boldsymbol{x}$ are considered to be realisations of $\widetilde{\boldsymbol{Y}}$ and $\boldsymbol{X}$, respectively, in a Bayesian setting. The starting point of this framework is to use Bayes' theorem to evaluate the probability of $\boldsymbol{x}$ knowing $\boldsymbol{y}$:

$$p(\boldsymbol{x}|\boldsymbol{y}) = \frac{p(\boldsymbol{y}|\boldsymbol{x}) p_{prior}(\boldsymbol{x})}{\int_{E^{N_{in}}} p(\boldsymbol{y}|\boldsymbol{x}') p_{prior}(\boldsymbol{x}') d\boldsymbol{x}'}, \tag{10}$$

where $\boldsymbol{y}$ represents the measurements of the outputs, $p_{prior}(\boldsymbol{x})$ is the supposed distribution of $\boldsymbol{x}$-values. In this formulation, the data are taken into account in the term $p(\boldsymbol{y}|\boldsymbol{x})$, the so-called likelihood. This represents the degree of belief of possible $\boldsymbol{x}$-values for a given set of measurement $\boldsymbol{y}$. These measurements deviate from the theoretical outputs obtained from realisations of Eq. (9). When assuming that the theoretical model is perfectly accurate and that the discrepancies only come from measurement errors, e.g., sensor noises, $\boldsymbol{y}$ can be written as follows:

$$\boldsymbol{y} = \widetilde{\boldsymbol{y}} + \boldsymbol{\eta}, \tag{11}$$

where components of $\boldsymbol{\eta}$ are supposed to be realisations of independent random variables, i.e, the measurement noise of two different outputs have no correlation. Subsequently, we assume that each component η_i of $\boldsymbol{\eta}$ is a realisation of a random variable that follows a Gaussian distribution p_η of zero-mean and σ-standard deviation. Consequently, the likelihood $p(\boldsymbol{y}|\boldsymbol{x})$ has the following expression:

$$p(\boldsymbol{y}|\boldsymbol{x}) = \prod_i p_\eta(y_i - \widetilde{y}_i(\boldsymbol{x})). \tag{12}$$

Combining Eqs. (10) and (12), the posterior distribution of the parameters $p(\boldsymbol{x}|\boldsymbol{y})$ is obtained and can be sampled efficiently with the Markov Chain Monte Carlo Method [33,34]. The most expensive part of the Bayesian method is to compute the likelihood in Eq. (12). This step requires to evaluate Eq. (9) over the parameter space. Instead of using sampling methods like Monte Carlo or latin-hypercube sampling, we replace here Eq. (9) by a surrogate:

$$\widetilde{\boldsymbol{Y}} = \sum_{\epsilon=0}^{N_o} \widetilde{\boldsymbol{Y}}_\epsilon \, \Psi_\epsilon(\boldsymbol{\theta}), \tag{13}$$

where all the uncertainties of $\boldsymbol{x}$ are gathered in a vector of random variables $\boldsymbol{\theta}$, and the Ψ's are the interpolants detailed in Section 2.1.2. In the APFEM, the coefficients $\widetilde{\boldsymbol{Y}}_\epsilon$ are naturally determined by solving Eq. (3) over the stochastic and physical space. By using APFEM instead of Monte Carlo and derivatives, one can accelerate the computation of the likelihood and consequently the derivation of the posterior distribution. Furthermore, by assuming here that the prior distribution is described by uniform random variables, no knowledge is required on the parameter space, except its vertices.

3. Applications

In the following, we first review two applications of APFEM of contemporary relevance on the parameter space evaluation of forward mechanical models. The second subsection focuses on APFEM as a tool for BI-based inverse problems.

3.1. APFEM for parameter space exploration

First, the mechanical response of a metamaterial actuator to a parametric input is studied. Second, the multi-directional buckling of a 3D beam, a highly nonlinear and discontinuous problem is solved.

3.1.1. Estimation of a metamaterial's behaviour

Metamaterials are a new class of materials showing superior performances—or at least "non-mainstream" properties—compared to traditional materials [35]. They have been the focus of an increased interest in the solid mechanics community due to their potential tunable high stiffness and strength-to-weight ratio [36]. These excellent properties arise from their designed geometry, consisting in units arranged in periodic patterns. Their manufacturing has become possible on an industrial scale thanks to the development of AM. Metamaterials have been extensively studied in virtually all fields of engineering applications [37,38]. Here, we build on the work of Bonfanti et al. for illustration purposes [39]. They performed a geometric optimisation of a lattice structure in combination with a machine learning layer framework. The target goal of the optimisation was the efficiency of the structure, defined as the ratio of the output displacement of a region of the structure to the input displacement of another region, see Fig. 1. This efficiency varies nonlinearly with respect to the input displacement. Instead of obtaining the output–input displacement curve by running repeated deterministic simulations with different values of input values, we apply here the APFEM for a given range of displacement, ranging from 0 to -10 (approximately 30% strain), see red arrow in Fig. 1. The metamaterial is modelled by a Saint Venant-Kirchhoff model with arbitrary deterministic Young's modulus and Poisson's ratio. We expect the problem to be smooth enough for a PCE of order 3 to give accurate results. The parameters of the APFEM static plane stress simulation are given in Table 1.

Baseline results were gathered using a single deterministic static finite element analysis with 10 time steps over which the input displacement of -10 is reached (i.e., by increment of -1). The simulation being static—as opposed to dynamic—the output at step n corresponds to a loading of $-n$. The evolution of the output displacement with input displacement is shown in Fig. 2 for both the baseline result (11 points) and the APFEM (continuous function of the displacement). For the latter, the output displacement was calculated by extracting from the stochastic nodal unknowns solved for (i.e., the $\boldsymbol{u}^{a\epsilon}$) the ones for the node of interest and reconstructing the function of the input parameter θ (here ramping from 0 to -10) through Eq. (1).

As expected, the output displacement is a nonlinear function of the input displacement, increasing with the absolute value of the input displacement. The APFEM continuous output matches perfectly the control points provided by the deterministic analysis. Remarkably, though no other information than the bounds of the input displacement are provided to the APFEM simulation, the framework is able to capture accurately all the intermediary loading conditions, i.e., the entire parameter space is explored with only one simulation.

Table 1
Geometrical features, finite element discretisation, boundary conditions and material parameters of the simulated metamaterial.

Parameters	Value
Geometrical features	height = 49, width = 61
Number of nodes	8,805
Type of elements	linear triangle
Number of elements	14,688
Range of displacement	0 to 10
Young's modulus and Poisson's ratio	1×10^7 Pa,0.3

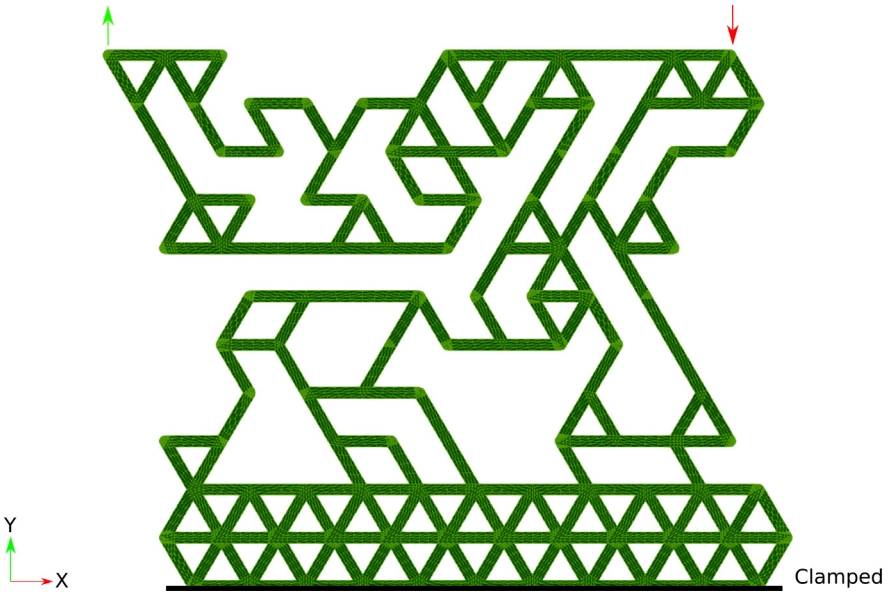

Fig. 1. Geometry of the metamaterial, taken from Ref. [39]. The bottom of the structure is clamped while a vertical displacement (red arrow) is imposed and a vertical output displacement (green arrow) is measured. (For interpretation of the references to colour in this figure legend, the reader is referred to the web version of this article.)

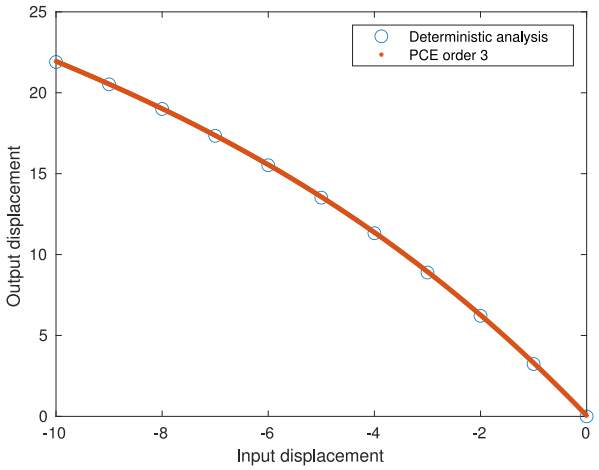

Fig. 2. Vertical output displacement vs. input displacement using APFEM and deterministic analysis.

Table 2
Geometrical features, finite element discretisation, boundary conditions and material parameters of the simulated beam buckling.

Parameters	Value
Geometrical features	length = 25, width = depth = 1
Number of nodes	1,336
Type of elements	quadratic tetrahedron
Number of elements	703
Range of lateral displacement	−0.1 to 0.1
Range of axial displacement	−0.2 to 0.2
Young's modulus and Poisson's ratio	1×10^7 Pa,0.4

3.1.2. Multi-directional buckling

Mechanical structures with high slenderness ratio can abruptly collapse under compressive loading. This phenomenon (known as buckling) has to be modelled accurately to evaluate precisely the reliability of a structural component. While all critical buckling loads and theoretical buckling modes can often be predicted by the theory [40], experimental instability often starts with a single local buckle [41]. Horton and Durham [42] concluded that geometrical imperfections are the main contributor to scatter in experimental values of buckling load when testing cylindrical shells. In this section, we focus on the stochastic buckling problem of a slender beam proposed by Ammouche and Jérusalem [12]. In that work, imperfections were introduced by a small deterministic lateral displacement, slightly distorting the beam to ensure buckling mode in one direction. A stochastic axial displacement was then applied spanning both compression and tension, demonstrating that the sharp variation of the lateral tip displacement with respect to axial displacement (increasing suddenly in compression due to buckling and remaining null in tension) was efficiently captured with the GSFEM [12].

Here, we revisit this problem by simultaneously considering a range of lateral displacement (both positive and negative) in the x-direction at the extremity of the beam (see Fig. 3(a)) and another range of displacement (both positive and negative) in the z-direction at the same extremity (see Fig. 3(b)), while clamping the other extremity. The lateral loading is first solved for, followed by the axial loading during which the lateral displacement constraints are released and measured. Note that both resolutions are done statically, meaning that the aim of the first loading is to introduce a bias in the second loading. The mechanical behaviour of the beam is modelled with a Saint Venant–Kirchhoff model. Three regimes are expected. When the axial displacement is tensile, no tip-displacement is observed. However, when the axial displacement is compressive enough, the beam will buckle either in the $+x$ or $-x$-direction depending on the introduced lateral displacement in the first load.

The aim of this study is to demonstrate that the APFEM can provide an accurate surrogate of the lateral displacement of the midpoint—a non-C^1 quantity of interest—with respect to a range of boundary conditions. To do so, we use wavelet interpolants, following Section 2.1.2.2 with $n = N = 1$, thus leading to a dimension of the stochastic space of 36. The finite element discretisation and the geometry are detailed in Table 2. The baseline comparison results are done by running 2500 Monte Carlo simulations with deterministic displacement inputs spanning the same ranges as the APFEM.

The APFEM results and Monte Carlo simulations are shown in Fig. 4. This example displays the capability of our method to capture pitchfork bifurcations in parametric studies. The wavelet interpolants capture with good accuracy the bifurcation point occurring near the transition between tensile and compressive displacement and the jump in tip displacement on both sides of the singularity. The fidelity of our surrogate could be further enhanced by adding more terms to the expansion, i.e, increasing the value of n and N in Eq. (7), though at a trade-off with computational time. Overall, the results show a very good ability for APFEM to capture singular problems by switching from PCE to wavelet interpolants. Note that the results shown here were done with 36 times more degrees of freedom (for the first order interpolants as $n = N = 1$) than a deterministic simulation. While this number might seem large (with important implications on computing memory required by the solver), it also needs to be compared to the potentially large number of Monte Carlo simulations one might require to capture the full spectrum of variation.

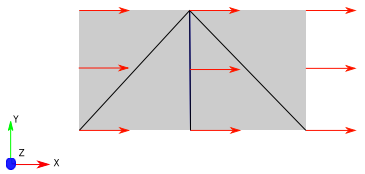

(a) A lateral "bias" (i.e., an imperfection) is first applied with a range of moderate lateral displacements in the x-direction.

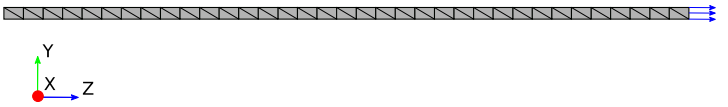

(b) A range of large axial displacement is applied in the z-direction.

Fig. 3. Multi-directionally loaded beam problem.

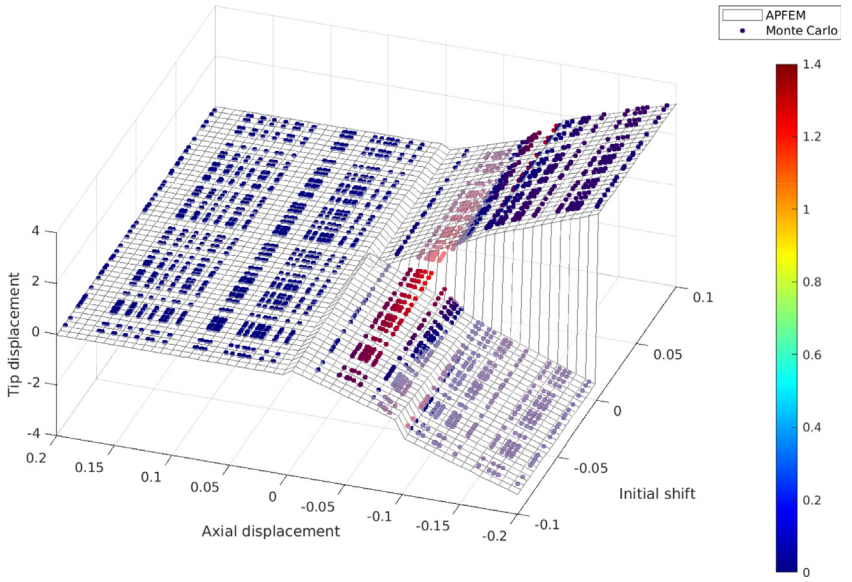

Fig. 4. Comparison of tip displacement values between Monte Carlo and APFEM using wavelet interpolants; the colour legend corresponds to the absolute error between APFEM and baseline Monte Carlo simulations.

Overall, APFEM is capable to capture important bifurcation problems such as the ones pertaining to material failure (e.g., buckling, fracture).

3.2. APFEM for inverse problems

In this section, we demonstrate how APFEM is particularly suitable for inverse problems such as inferences. We focus particularly on the identification of constitutive properties of mechanical components from the knowledge of a set of measurements (e.g., experimental). We first apply APFEM to contact mechanics for the determination of a friction coefficient in the Cattaneo–Mindlin problem, and then infer the stiffness of a fictitious brain tumour from midline shift measurements arising during cardiac cycle tissue deformation.

3.2.1. Contact mechanics: The Cattaneo–Mindlin problem

Virtually all engineering structures with moving parts do involve contacts. These contacts can result in nucleation of cracks and eventually failure. The problem, in addition to being complex from a theoretical standpoint, is also constrained in its experimental monitoring, relying on external observations when potential issues arise within the (inaccessible) contact area. We propose here to use BI in conjunction with APFEM to approach this challenge.

3.2.1.1. Theoretical framework. In most finite element frameworks, solving contact mechanics problems requires the discretisation of one or all bodies in contact and the computation of the distance between the nodes or the element faces of the surfaces in contact. Coupling these algorithms with APFEM is outside the scope of our study. Instead, we simulate contact between a spherical object and a plane by making use of the analytical approaches developed by Cattaneo and Mindlin [43,44] for partial slip Hertzian contact, see Fig. 5(a). This approach has been used for fretting analysis in roller bearings [45] in turbines but also in biomechanics for prosthetic hip bearings [46]. Cattaneo and Mindlin independently derived the distribution of normal and tangential loading distributions when a sphere is pressed into a half space. In the case where the total normal and tangential forces applied in the half space are P and Q, respectively, their spatial distribution p and q can be written as:

$$p(r) = p_0\sqrt{1-\frac{r^2}{a^2}} \text{ if } 0 \leq r \leq a, \tag{14}$$

$$q(r) = \begin{cases} \mu p_0 \left(\sqrt{1-\frac{r^2}{a^2}} - \frac{c}{a}\sqrt{1-\frac{r^2}{c^2}} \right) & \text{if } 0 \leq r \leq c \\ \mu p(r) & \text{if } c \leq r \leq a, \end{cases} \tag{15}$$

where a is the radius of contact, c the length of the stick zone, μ the friction coefficient, r the radial coordinate of the material point and p_0 a normalised pressure at the centre of the contact surface ($r = 0$), see Fig. 5(a). The stick zone radius c depends nonlinearly on the friction coefficient and the external forces:

$$c = a\left(1-\frac{Q}{\mu P}\right)^{\frac{1}{3}}. \tag{16}$$

Here, our aim is to evaluate the value of the unknown friction coefficient through the sole observation of the contact's outer boundary. In the APFEM framework, the friction coefficient is taken to be an unknown parameter. Because Eq. (16) is a power function of μ, the evaluation of the stick zone size's distribution is not straightforward. One can however do so by solving a differential equation through a method proposed by Debusschere et al. [11]; see Appendix for more details on its use for Eq. (16). In our approach, the uncertainty of the contact is modelled by an uncertainty on the Neumann boundary conditions. Indeed, while the normal pressure p is applied deterministically, it is not the case for the tangential pressure as its treatment differs whether the material point at a radius r is inside the stick zone or in the slip zone, see Eq. (15). Similarly, a direct evaluation of the term $\sqrt{1-\frac{r^2}{c^2}}$ is also impractical as the content of the square root can have non-zero probability of being negative, and the condition $c \leq r$ is not uniquely defined as r is a deterministic quantity while c is a probability distribution. Here, we approximate the inequality of Eq. (15) as follows:

$$q(r) = \begin{cases} \mu p_0 \left(\sqrt{1-\frac{r^2}{a^2}} - \frac{c}{a}\sqrt{1-\frac{r^2}{c^2}} \right) & \text{if } 0 \leq r \leq c_{inf} \\ \mu p_0 \left(\sqrt{1-\frac{r^2}{a^2}} - \frac{c}{a}\tilde{f}(\frac{r}{c}) \right) & \text{if } c_{inf} \leq r \leq c_{sup} \\ \mu p(r) & \text{if } c_{sup} \leq r \leq a, \end{cases} \tag{17}$$

where c_{inf} and c_{sup} are respectively the inferior and superior bounds of c. The second term of the first line of the equation is calculated making use of Appendix. In the second line, however, the square root is replaced by the function $\tilde{f}(x) = -52 + 162.6x - 114.93x^2 - 92.1x^3 + 141.47x^4 - 44.96x^5$, which is a polynomial approximation of $\sqrt{1-x^2}$ in [0.763,1.31], corresponding to $[\frac{c_{inf}}{c_{sup}}, \frac{c_{sup}}{c_{inf}}]$ with the values used in this example. This change in Eq. (15) is required as the probability of $1-\frac{r^2}{c^2}$ of being negative is non-zero when $r \in [c_{inf}, c_{sup}]$. While this is in fact not strictly an issue when using the algorithm in Appendix to compute square root of stochastic quantities, it introduces additional errors that can be avoided by use of the proposed polynomial approximation along with the usual stochastic operations for polynomials. We emphasise that Eq. (17) still, however, introduces irreversible modifications on Eq. (15). Hence, the Monte Carlo solution cannot be expected to be fully recovered, even with high order PCE, as the problem solved in the deterministic and stochastic framework are not completely equivalent, similarly to what Rosic et al. noted when extending intrusive stochastic methods to plasticity [47].

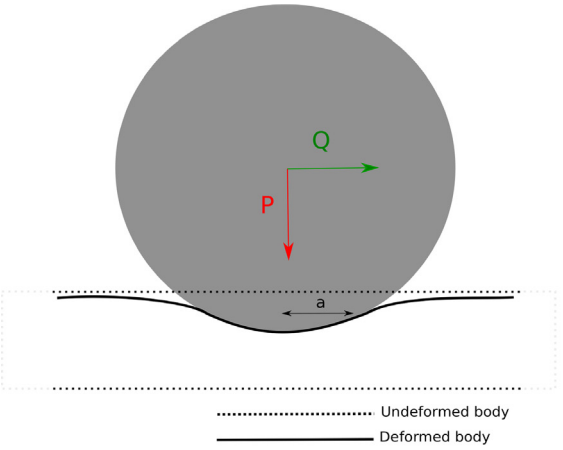

(a) Simplified scheme of the Hertzian contact problem.

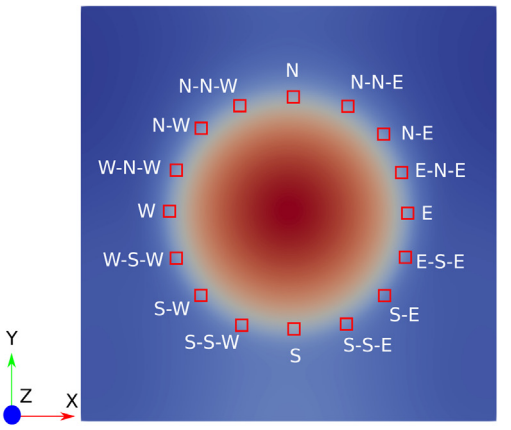

(b) 2D view of the FE contact problem and measurement points for BI.

Fig. 5. Cattaneo–Mindlin problem.

3.2.1.2. Application. Here, the contact problem is idealised by pressing normally a spherical object into a hyperrectangle, and dragging it over its surface. By only modelling the half-plane where the contact is taken into account through boundary conditions, we aim to determine the friction coefficient using measurements of the x-displacement of material points located at the edge of the contact surface, see Fig. 5(b). The material behaviour of the half-plane is modelled by a Saint-Venant Kirchhoff constitutive model. The geometrical features, finite element discretisation and constitutive model material parameters are given in Table 3. Finally, we assume that the prior distribution of the friction coefficient is a uniform distribution between 0.3 and 0.4.

We use *in silico* data to simulate an external set of measurements (e.g., of experimental nature). This is done by performing a deterministic simulation with a friction coefficient equal to 0.35, gathering the x-displacements of the cardinal points (see Fig. 5(b)), and artificially "polluting" these measurements (as could be expected from experimental measurements) with a noise following a Gaussian distribution centred in 0 with a standard deviation of 5.10^{-5} to generate the vector of measurements $\boldsymbol{y}$, see Eq. (11). Taking the prior distribution of friction coefficient to be uniform between 0.3 and 0.4, the likelihood of Eq. (12) can then be computed, eventually leading to the posterior distribution of the friction coefficient through Eq. (10) using APFEM with order 4 PCE.

Fig. 6 shows the comparison between the true value of the friction coefficient and the posterior distribution after BI with various level of measurement knowledge defined by (a) two measurement points (W and E), (b) four measurement points (W, N, E and S), (c) eight measurement points (W, N-W, N, N-E, E, S-E, S, S-W) and (d) sixteen measurements (W, W-N-W, N-W, N-N-W, N, N-N-E, N-E, E-N-E, E, E-S-E, S-E, S-S-E, S, S-S-W, S-W, W-S-W). As expected, the greater the number of measurements, the narrower the posterior distribution is. However, the maximum value of the posterior distribution is converging towards approximately 0.355, i.e., an error $e = 0.005$ with respect to the original deterministic model defined with $\mu = 0.35$ (a 1.4% error). Again, this discrepancy was expected, as Eq. (15) had to be approximated for our stochastic framework to be leveraged. While this theoretical approximation hampers the accuracy of our framework for complex relationships between parameters and boundary conditions, the predicted distribution of the friction coefficient remains remarkably close to the original values with a relatively low number of measurements: four measurements of the outer boundary of the contact area are enough to estimate the friction coefficient within $\sim 2\%$ of error.

3.2.2. Brain mechanics: A large scale problem

This section illustrates the flexibility of the BI-APFEM framework for large scale simulations ($>$ 1 million degrees of freedom) with an application involving brain mechanics modelling.

Clinicians have traditionally been using the measurement of midline shift (MLS)—the topological line separating left and right hemispheres, readily observable through common imaging techniques—as an indicator of structural movement and tool for surgical decision-making, in particular in the context of stroke. Here, we borrow the

Table 3
Geometrical features, finite element discretisation, boundary conditions and material parameters of the contact simulation.

Parameters	Value
Geometrical features	Length = width = 10, depth = 2
Number of nodes	59,049
Type of elements	quadratic tetrahedron
Number of elements	52,000
Total normal force	8×10^5 N
Total friction force	2×10^5 N
Young's modulus and Poisson's ratio	1×10^6 Pa, 0.3

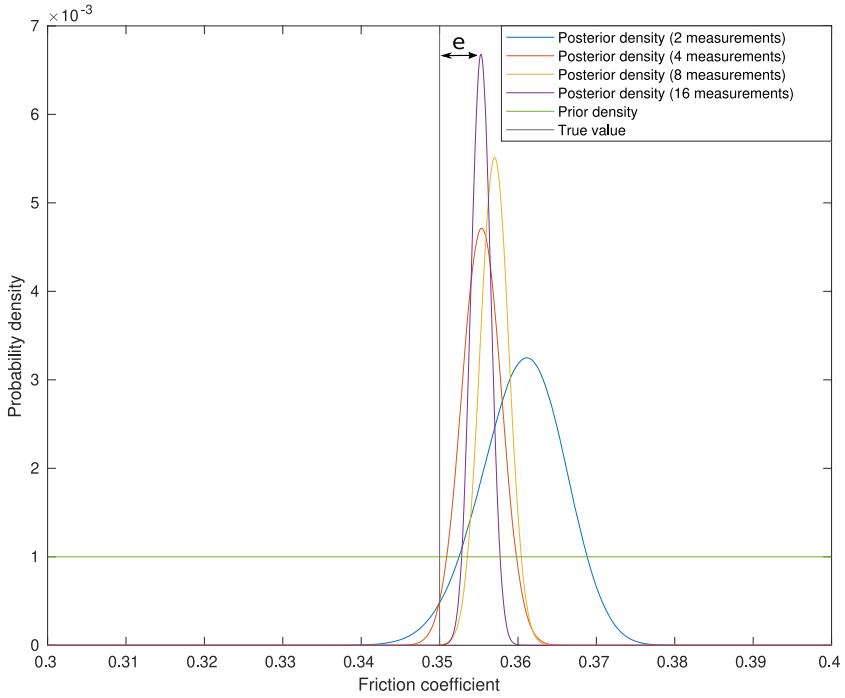

Fig. 6. Prior and posterior distributions of the friction coefficient.

simulation framework of Bing et al. [48] to infer from MLS measurements the stiffness of a brain tumour creating an asymmetrical brain deformation during a pressure rise in the arteries. In this work, a finite element human head was created using MRI and magnetic resonance angiography, see Ref. [48] for more details. The model includes vasculature, brain organs and skulls. We use a Neo-Hookean model to simulate the mechanical behaviour of the brain components as a first approximation. The parameters of the constitutive model (adapted from the same reference to a Neo-Hookean model) are detailed in Table 4 while the details of the finite element discretisation are given in Table 5. Here, we arbitrarily assume that a tumour in the temporo-parietal region of the left hemisphere has an increased stiffness, and that an arbitrary increase of blood pressure of 100 Pa (applied on the inside of the vasculature; note that we only use a fraction of what would be expected from the rise of pressure in the vasculature during a cardiac cycle) coupled to the presence of this mass leads to a small MLS, see Fig. 7. Note that, while theoretically possible, the clinical relevance of this hypothetical method is by no means demonstrated here; it is merely used here as an illustrative example of BI-APFEM in large scale problems.

Similarly to the contact mechanics problem, we use an *in silico* experiment to generate "experimental" measurement data of the MLS by: (i) gathering MLS-values through a deterministic simulation with an arbitrary tumour's Young's modulus of 13021 Pa, see Figs. 7(a) and 7(c); and (ii) "polluting" these values with a Gaussian

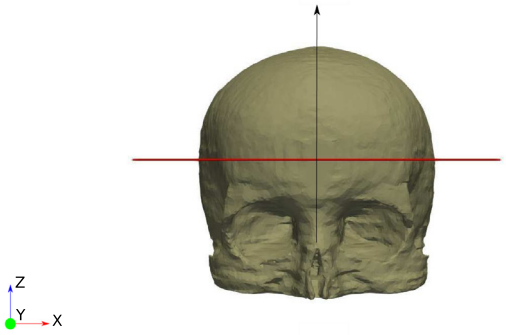

(a) 3D Head model. In red, the plane where the MLS values are acquired.

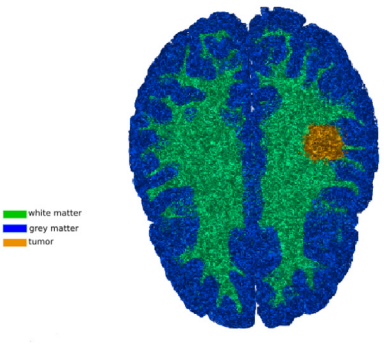

(b) Horizontal meshed section of the brain showing tumour in the temporo-parietal region of the left hemisphere.

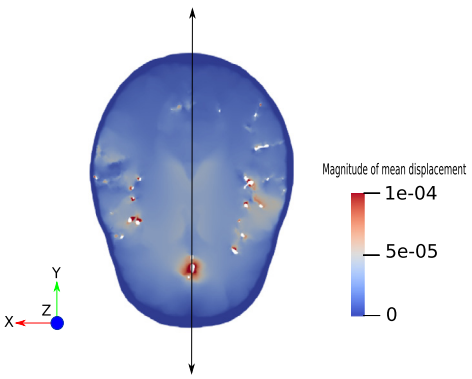

(c) Horizontal section for one deterministic simulation. The black line indicates the midline. The displacement field is provided as an illustration for the case of a tumour's Young's modulus of 13021 Pa.

Fig. 7. 3D head model and section used for gathering of MLS data.

Table 4
Material parameters of the brain (the skull is assumed rigid).

Brain components	Young's modulus	Poisson's ratio
White matter/Brainstem	1.302×10^4 Pa	0.45
Grey matter/Cerebellum	2.958×10^3 Pa	0.45
Falx	3.15×10^7 Pa	0.45
Ventricle	2.90×10^2 Pa	0.45
Tumour	from 12.37 kPa to 13.67 kPa	0.45

noise of null mean value and standard deviation of 4.10^{-10}, supposed to be independent for each measurement. Making use of BI-APFEM with second order PCE with a Young's modulus ranging from 12.37 kPa to 13.67 kPa, the measurements allow the computation of the likelihood of the Young's modulus of the tumour, see Eq. (12), and eventually its probability distribution. As shown on Fig. 8, the posterior distribution converges to the true value with a good accuracy from five experimental MLS measurements onwards.

4. Discussion

In this work, we specialised the previously proposed GSFEM to uniform distribution to allow for an *a posteriori* parametric control of input parameters solely defined by their bounds: the APFEM. Doing so, we leverage the

Table 5
Finite element discretisation parameters of the brain mechanics simulation.

Parameters	Value
Number of nodes	344,872
Type of elements	linear tetrahedron
Number of elements	1,952,523
Pressure	100 Pa

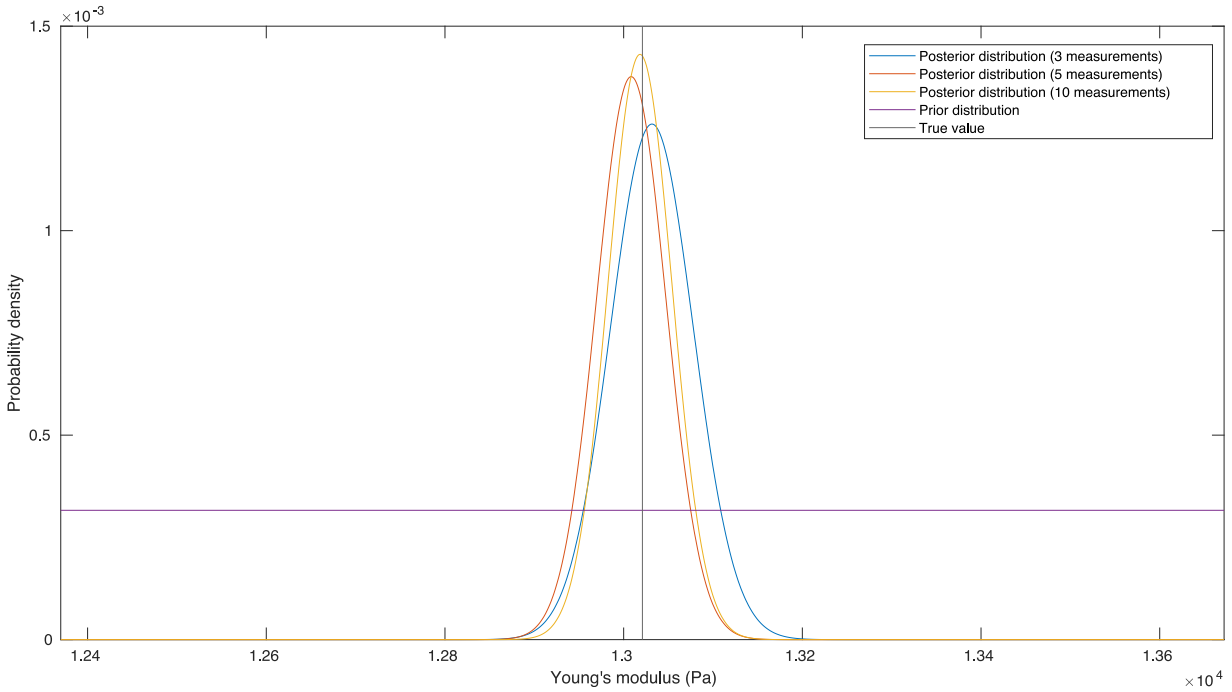

Fig. 8. Prior and posterior distributions of the tumour's Young's modulus.

flexibility and algebraic libraries of GSFEM for parametric studies, i.e., without the need for multiple simulations (e.g., Monte Carlo) and with the same precision as with deterministic simulations. Another obvious advantage is that the identification of the bounds of the unknown parameters can realistically be measured or inferred experimentally with cost-effective experiments; as opposed to the original GSFEM that requires a knowledge of the overall distribution. This simplification comes at the cost of losing the ability of GSFEM to retrieve outputs probability distribution as the uniform distributions used for input parameters do not represent the real distribution of the entry random variables. However, as the uniform distribution provides an even weight at each point of the parameter domain, APFEM captures accurately the response of the system for every input in that bounded space (as opposed to, e.g., Gaussian distributions where the low probabilities of events in the tails of the distribution can lead to higher errors in GSFEM [12]). Furthermore, the use of bounds in APFEM naturally allows for the exploration of "worst case scenarios" similarly to interval methods, but—unlike the latter—with the additional benefit of capturing exactly the parameter space in-between. Overall, the APFEM is ideally conceived for design planning and parametric analysis as demonstrated through our first two applications, and in particular the buckling example where a pitchfork-bifurcation could be captured with wavelet interpolants.

One direct corollary for these features is that APFEM can be used for BI. Note that the general formulation of GSFEM does not lend itself as easily to BI as uniform prior distribution is required for the computation of the likelihood in Eq. (12) over the whole parameter space. Indeed, other prior distributions are bound to introduce errors in the surrogate provided by GSFEM for the points lying in the medium–low probability region [30]. The

resulting BI-APFEM, however, is able to infer rapidly unknown parameter values with a low number external experimental measurements and without the need for further simulations after the initial APFEM simulation has been done. This impressive flexibility needs to be tempered by the need to derive constitutive models in the stochastic space through the algebra proposed previously by Ammouche and Jérusalem [12]. Here, we used the stochastic Saint-Venant Kirchhoff model for simplicity, but other models could easily be developed. The contact mechanics example showed here highlights the difficulty that one can encounter when using power-law in the stochastic space. While some methods can be used (see Appendix) to do those operations, they might come with approximations eventually leading to the type of errors observed in the third application presented here. When the operations remain straightforward, the method can show its full potential, as shown in the fourth brain mechanics application.

Both our APFEM and BI-APFEM still suffer from important limitations. The current implementation only takes into account space-independent random variables while more realistic simulations might include random fields exhibiting spatial correlation. In addition, the APFEM requires additional stochastic degrees of freedom, hence increasing the size of the problem. Consequently, using APFEM when the counterpart deterministic problems are already large can become very quickly computationally expensive, with the caveat that only one simulation is required. We argue however, that with careful programming, one can simulate large problems such as the last problem in this paper where 40 cores were used to simulate a problem with approximately $\sim$2.5 millions degrees of freedom ($\sim$300,000 nodes $\times$ 3 dimensions $\times$ 3 stochastic degrees of freedom) within a few hours. Finally, avoiding the intrusive character of our approach could be done with non-intrusive PCE methods, where the coefficients of the expansions are determined with different schemes, e.g., least-square regression, though at the cost of a lack of robustness as increasing the number of sampled points does not necessarily lead to convergence [49].

5. Conclusion

Here, we proposed the APFEM, an intrusive method for efficient parameter exploration with the sole knowledge of parameter bounds. The method leverages the flexibility of GSFEM and can readily be extended to many problems. It can also be used in conjunction with BI, without the need for further simulations. Ongoing work involves extending the APFEM to stochastic geometrical features. This will allow further enhancement of the design step in the engineering process as one simulation will then give a precise estimate of different geometries' performances.

Declaration of competing interest

The authors declare that they have no known competing financial interests or personal relationships that could have appeared to influence the work reported in this paper.

Data availability

The software is available under academic license on https://github.com/muphisim.

Acknowledgement

The authors acknowledge funding by the EPSRC Prosperity Partnership Grant EP/S005072/1. The authors also thank Alice Collier and Van Dung Nguyen for their help with the meshing of the head model.

Appendix

This appendix details the stochastic operations needed in Section 3.2.1.2. They involve non-polynomial operations of random variables such as square root or cubic root. A Taylor expansion, albeit simpler to compute, requires a high number of terms to obtain correct accuracy and is valid only in the vicinity of the centre of the expansion. Hence, we build on the work of Debusschere et al., where a methodology for non-polynomial operation on random quantities is proposed [11].

A.1. Algorithm for computation of non-polynomial functions of random variables

We briefly summarise the integration approach for non-polynomial function evaluations proposed by Debusschere et al. [11]. Let us consider a parametrised function u of a variable x and its derivative g, all defined in a stochastic space with stochastic variable θ, with:

$$x = x(s,\theta) = \sum_{j=0}^{P} x_j(s)\,\Psi_j(\theta), \tag{18}$$

$$u = u(s,\theta) = \sum_{j=0}^{P} u_j(s)\,\Psi_j(\theta), \tag{19}$$

$$g = g(s,\theta) = \sum_{j=0}^{P} g_j(s)\,\Psi_j(\theta), \tag{20}$$

where $P+1$ is the dimension of the stochastic space, and s parametrises the "path" across the space of PCE coefficients. Consequently, we can write:

$$\int_{s_1}^{s_2} \frac{\partial u}{\partial s} ds = \int_{s_1}^{s_2} g \frac{\partial x}{\partial s} ds. \tag{21}$$

Following Galerkin projections and additional mathematical steps detailed by Debusschere et al. [11], Eq. (21) leads to:

$$u_k(s_2) - u_k(s_1) = \sum_{j=0}^{P} \int_{x_j(s_1)}^{x_j(s_2)} \sum_{i=0}^{P} C_{ijk} g_i dx_j, \ \forall k \in [0, P], \tag{22}$$

where C_{ijk} is a third order tensor equal to $\langle \Psi_i \Psi_j, \Psi_k \rangle$. We now take $x_j(s)$ as having the form $x_j(s) = (a_j - \tilde{a}_j)s + \tilde{a}_j$, where $\tilde{a}_j$ is assumed to be known by taking $\tilde{a} = \sum_{j=0}^{P} \tilde{a}_j \Psi_j$ as a deterministic value (i.e., only $\tilde{a}_0$ is non-zero). Similarly, we assume that u is easily evaluated at this point. $a = \sum_{j=0}^{P} a_j \Psi_j$ is stochastic and known but the evaluation of u at this point is unknown. One can then rewrite Eq. (22) as follows:

$$u_k(s_2) - u_k(s_1) = \sum_{j=0}^{P} (a_j - \tilde{a}_j) \int_{s_1}^{s_2} \sum_{i=0}^{P} C_{ijk} g_i ds. \tag{23}$$

With a change of variable where s_1 is replaced by 0 and s_2 by s', one has:

$$u_k(s') - u_k(0) = \sum_{j=0}^{P} (a_j - \tilde{a}_j) \int_{0}^{s'} \sum_{i=0}^{P} C_{ijk} g_i ds. \tag{24}$$

We now differentiate this equation with respect to s'. Taking into account that $u_k(0)$ is independent of s', we obtain the following equation:

$$\dot{u}_k(s') = \sum_{j=0}^{P} (a_j - \tilde{a}_j) \sum_{i=0}^{P} C_{ijk} g_i(s'). \tag{25}$$

The aim of the method is to compute $u_k(1)$ iteratively for all k between 0 and P with the sole original knowledge of $u_k(0)$. To this end, one can thus use Eq. (25) to write:

$$u_k(s' + ds') = u_k(s') + \dot{u}_k(s')ds' = u_k(s') + \sum_{j=0}^{P} (a_j - \tilde{a}_j) \sum_{i=0}^{P} C_{ijk} g_i(s')ds'. \tag{26}$$

As $u_k(0)$ is trivial to evaluate (it is the stochastic component k of the function u evaluated at the deterministic point $\tilde{a}$), making use of this iterative scheme to compute $u_k(s' + ds')$ only requires the knowledge of $g_i(s')$ from $u_k(s')$. The procedure is summarised in Algorithm 1.

Algorithm 1 Evaluation of a non-linear function u for a random variable a

1: **Initialisation**. Set $s \leftarrow 0$. Set value of step increment ds, evaluate $u(\tilde{a})$ and $g(\tilde{a})$.
2: **while** $s \neq 1$ **do**
3: For k=0 to P, evaluate $u_k(s + ds)$ with Eq. (26).
4: For k=0 to P, evaluate and store $g_k(s)$ from the knowledge of $u(s)$.
5: Set $s \leftarrow s + ds$
6: **end while**

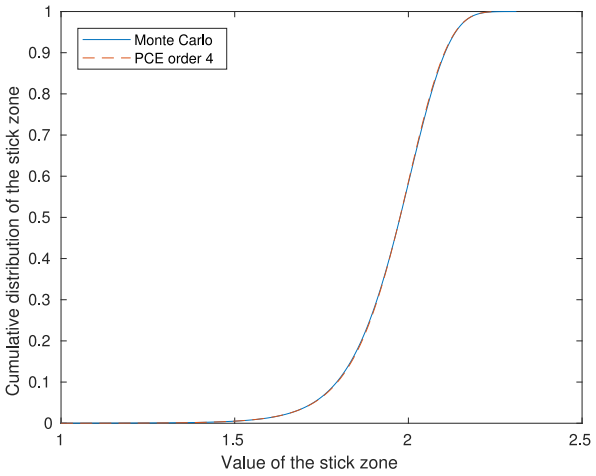

Fig. 9. Comparison of the stick zone radius CDF between Monte Carlo method and PCE approximation of order 4 following the proposed algorithm.

A.2. Application to power 1/3

In this section, a function $u(x) = x^{1/3}$ is considered. Trivially, one has $g(x) = \frac{1}{3}x^{-2/3}$, which can thus be rewritten as:

$$g(x) = \frac{1}{3}\frac{u(x)}{x}. \tag{27}$$

Here, it is possible to compute $g(x)$ if $u(x)$ is known as the division of two random variables is an operation that can be easily done, see Appendix of Ammouche and Jérusalem [12] for more details. Consequently, Eq. (26) becomes:

$$u_k(s' + ds') = u_k(s') + \frac{1}{3}(a_j - \tilde{a}_j)\sum_{j=0}^{P}\sum_{i=0}^{P} C_{ijk}\left(\frac{u(s')}{x(s')}\right)ds'. \tag{28}$$

For illustrative purposes, this algorithm is used here for Eq. (16), with a value of $\frac{Q}{P}$ is equal to 0.25, and where the friction coefficient μ is a random gaussian variable centred in 0.35 with a standard deviation of 0.025. We also use a step $ds' = 0.001$ for the discretisation of Eq. (26). Fig. 9 shows the CDF of c-values in Eq. (16) using Monte Carlo and a PCE approximation of order 4, showing a good performance. Similarly, this algorithm also allows for the computations of square roots in Eq. (17).

References

[1] M. Khosravani, Composite materials manufacturing processes, Appl. Mech. Mater. 365 (2011) 110–116.
[2] N. Korshunova, I. Papaioannou, S. Kollmannsberger, D. Straub, E. Rank, Uncertainty quantification of microstructure variability and mechanical behavior of additively manufactured lattice structures, Comput. Methods Appl. Mech. Engrg. 385 (2021) 114049.
[3] R. Caflisch, Monte Carlo and quasi-Monte Carlo methods, Acta Numer. 7 (1998) 1–49.
[4] N. Weiner, The homogeneous chaos, Amer. J. Math. 60 (4) (1938) 897–936.

[5] D. Xiu, G. Karniadakis, The Wiener-Askey polynomial chaos for stochastic differential equations, SIAM J. Sci. Comput. 24 (2002) 619–644.
[6] K. Sepahvand, S. Marburg, Spectral stochastic stochastic finite element method in vibroacoustic analysis of fiber-reinforced composites, Procedia Eng. 199 (2017) 1134–1139.
[7] B. Sudret, A. der Kiureghian, A. Stochastic finite elements and reliability: a state-of-the-art report, 2000, pp. 1–173.
[8] S. Huang, M. Sankaran, R. Ramesh, Collocation-based stochastic finite element analysis for random field problems, Probab. Eng. Mech. 22 (2007) 194–205.
[9] M. Eiermann, O. Ernst, E. Ullmann, Computational aspects of the stochastic finite element method, Comput. Vis. Sci. 10 (2007) 3–15.
[10] G. Stefanou, The stochastic finite element method: Past present and futures, Comput. Methods Appl. Mech. Engrg. 1998 (2009) 1031–1051.
[11] B. Debusschere, H. Najm, P. Pebay, Numerical challenges in the use of polynomial chaos representations for stochastic processes, Soc. Ind. Appl. Math. 26 (2) (2004) 698–719.
[12] Y. Ammouche, A. Jérusalem, A modular nonlinear stochastic finite element formulation for uncertainty estimation, Comput. Methods Appl. Mech. Engrg. 396 (2022) 115044.
[13] O. Le Maitre, O. Knio, H. Najm, R. Ghanem, Uncertainty propagation using Wiener–Haar expansions, J. Comput. Phys. 197 (2004) 28–57.
[14] D. Moens, M. Hanss, Non-probabilistic finite element analysis for parametric uncertainty treatment in applied mechanics: Recent advances, Finite Elem. Anal. Des. 47 (1) (2011) 4–16.
[15] M. Faes, D. Moens, Recent trends in the modeling and quantification of non-probabilistic uncertainty, Arch. Comput. Methods Eng. 27 (2019) 633–671.
[16] S. Rao, L. Berke, Analysis of uncertain structural systems using interval analysis, AIAA J. 35 (1997).
[17] M. Modares, R. Mullen, R. Muhanna, Natural frequencies of a structure with bounded uncertainty, J. Eng. Mech. 132 (2006).
[18] X. Long, C. Jiang, K. Liu, X. Han, W. Gao, B. Li, An interval analysis method for fatigue crack growth life prediction with uncertainty, Comput. Struct. 210 (2018) 1–11.
[19] M. Xu, Z. Qiu, A dimension-wise method for the static analysis of structures with interval parameters, Sci. China Phys. Mech. Astron. 57 (2014) 1934–1945.
[20] B. Ni, C. Jiang, Interval field model and interval finite element analysis, Comput. Methods Appl. Mech. Engrg. 360 (2020) 112713.
[21] T. Kirchdoerfer, M. Ortiz, Data-driven computational mechanics, Comput. Methods Appl. Mech. Engrg. 304 (2016) 81–101.
[22] K. Karapiperis, M. Ortiz, J. Andrade, Data-Driven nonlocal mechanics: Discovering the internal length scales of materials, Comput. Methods Appl. Mech. Engrg. 386 (2021) 114039.
[23] P. Carrara, M. Ortiz, L. De Lorenzis, Data-driven rate-dependent fracture mechanics, J. Mech. Phys. Solids 155 (2021) 104559.
[24] H. Salahshoor, M. Ortiz, Model-free data-driven viscoelasticity in the frequency domain, 2022, http://dx.doi.org/10.48550/ARXIV.2205.06674, URL https://arxiv.org/abs/2205.06674.
[25] E. Konukoglu, J. Relan, U. Cilingir, B. Menze, P. Chinchapatnam, A. Jadidi, H. Cochet, M. Hocini, H. Delingette, P. Jaïs, M. Haïssaguerre, N. Ayache, M. Sermesant, Efficient probabilistic model personalization integrating uncertainty on data and parameters: Application to eikonal-diffusion models in cardiac electrophysiology, Prog. Biophys. Mol. Biol. 107 (1) (2011) 134–146.
[26] K. Linka, A. Schafer, X. Meng, Z. Zou, G. Karniadakis, E. Kuhl, Bayesian Physics-Informed Neural Networks for real-world nonlinear dynamical systems, 2022.
[27] M. Mohamedou, K. Zulueta, C.N. Chung, H. Rappel, L. Beex, L. Adam, A. Arriaga, Z. Major, L. Wu, L. Noels, Bayesian identification of Mean-Field Homogenization model parameters and uncertain matrix behavior in non-aligned short fiber composites, Compos. Struct. 220 (2019) 64–80.
[28] H. Rappel, L. Beex, J.S. Hale, L. Noels, S.P.A. Bordas, A tutorial on Bayesian inference to identify material parameters in solid mechanics, Arch. Comput. Methods Eng. 27 (2020) 361–385.
[29] B. Rosić, A. Kučerová, J. Sýkora, O. Pajonk, A. Litvinenko, H. Matthies, Parameter identification in a probabilistic setting, Eng. Struct. 50 (2013) 179–196.
[30] Y. Marzouk, H. Najm, L. Rahn, Stochastic spectral methods for efficient Bayesian solution of inverse problems, J. Comput. Phys. 224 (2) (2007) 560–586.
[31] R. Cameron, W. Martin, Transformations of Wiener integrals under translations, Ann. of Math. 45 (1944) 386–396.
[32] B. Alpert, A class of bases in L 2 for the sparse representation of integral operators, SIAM J. Math. Anal. (1993) 246–262.
[33] C. Geyer, Practical Markov chain Monte Carlo, Statist. Sci. 7 (1996) 473–483.
[34] W. Gilks, S. Richardson, Markov chain Monte Carlo in practice, Chapman and Hall, 1996.
[35] X. Zheng, H. Lee, T. Weisgraber, M. Shusteff, J. DeOtte, E. Duoss, J. Kuntz, M. Biener, Q. Ge, J. Jackson, S. Kucheyev, N. Fang, C. Spadaccini, Ultralight, ultrastiff mechanical metamaterials, Science 344 (6190) (2014) 1373–1377.
[36] X. Yu, J. Zhou, H. Liang, Z. Jiang, L. Wu, Mechanical metamaterials associated with stiffness, rigidity and compressibility: A brief review, Prog. Mater. Sci. 94 (2018) 114–173.
[37] R. Hasan, R. Mines, A.R. A.W., E. Shen, S. Tsopanos, W. Cantwell, W. Brooks, C. Sutcliffe, Comparison of the drop weight impact performance of sandwich panels with aluminium honeycomb and titanium alloy micro lattice cores, 24 (2010) 413–418.
[38] S. Ahmadi, G. Campoli, A. Yavari, S. Sajadi, R. Wauthle, J. Schrooten, H. Weinans, A. Zadpoor, Mechanical behavior of regular open-cell porous biomaterials made of diamond lattice unit cells, J. Mech. Behav. Biomed. Mater. 34 (2014) 106–115.
[39] S. Bonfanti, R. Guerra, F. Font-Clos, D. Rayneau-Kirkhope, S. Zapperi, Automatic design of mechanical metamaterial actuators, Nature Commun. 11 (1) (2020).
[40] H. Leipholz, J. Hutchinson, Theory of Elasticity, J. Appl. Mech. 42 (4) (1975) 911.

[41] B. Pan, W. Cui, An overview of buckling and ultimate strength of spherical pressure hull under external pressure, Mar. Struct. 23 (3) (2010) 227–240.
[42] W. Horton, S. Durham, Imperfections, a main contributor to scatter in experimental values of buckling load, Int. J. Solids Struct. 1 (1) (1965) 59–72.
[43] C. Cattaneo, Sul contatto de due corpi elastici: Distribuzione locale deglisforzi, in: Rendiconti dell'Accademia Nazionale dei Lincei, vol. 6, 1938, pp. 342–349.
[44] R. Mindlin, Compliance of elastic bodies in contact, 1949.
[45] S. Lin, J. Sun, Y. Peng, Analysis of axial fretting mode and mechanical model for a four-row tapered roller bearing, Int. J. Mech. Sci. 228 (2022) 107463.
[46] A. Sanders, R. Brannon, Assessment of the applicability of the hertzian contact theory to edge-loaded prosthetic hip bearings, J. Biomech. 44 (16) (2011) 2802–2808.
[47] B. Rosić, M. Hermann, Variational theory and computations in stochastic plasticity, Arch. Comput. Methods Eng. 22 (2015) 457–509.
[48] Y. Bing, D. Garcia-Gonzalez, N. Voets, A. Jérusalem, Medical imaging based in silico head model for ischaemic stroke simulation, J. Mech. Behav. Biomed. Mater. 101 (2020) 103442.
[49] G. Blatman, B. Sudret, Adaptive sparse polynomial chaos expansion based on least angle regression, J. Comput. Phys. 230 (6) (2011) 2345–2367.